ACS central science

Research Article

http://pubs.acs.org/journal/acscii

Close Correlation of Monoamine Oxidase Activity with Progress of Alzheimer's Disease in Mice, Observed by *in Vivo* Two-Photon Imaging

Dokyoung Kim,[†,‡,§] Sung Hoon Baik,[∥,§] Seokjo Kang,[∥] Seo Won Cho,[†] Juryang Bae,[†] Moon-Yong Cha,[∥] Michael J. Sailor,[‡] Inhee Mook-Jung,*[,∥] and Kyo Han Ahn*[,†]

[†]Department of Chemistry, Pohang University of Science and Technology (POSTECH), 77 Cheongam-Ro, Nam-Gu, Pohang, Gyungbuk 37673, Republic of Korea

[‡]Department of Chemistry and Biochemistry, University of California, San Diego, La Jolla, California 92093, United States

[∥]Department of Biochemistry and Biomedical Sciences, College of Medicine, Seoul National University, 103 Daehak-Ro, Jongro-Gu, Seoul 110-799, Republic of Korea

Supporting Information

ABSTRACT: Monoamine oxidases (MAOs) play an important role in Alzheimer's disease (AD) pathology. We report *in vivo* comonitoring of MAO activity and amyloid-β (Aβ) plaques dependent on the aging of live mice with AD, using a two-photon fluorescence probe. The probe under the catalytic action of MAO produces a dipolar fluorophore that senses Aβ plaques, a general AD biomarker, enabling us to comonitor the enzyme activity and the progress of AD indicated by Aβ plaques. The results show that the progress of AD has a close correlation with MAO activity, which can be categorized into three stages: slow initiation stage up to three months, an aggressive stage, and a saturation stage from nine months. Histological analysis also reveals elevation of MAO activity around Aβ plaques in aged mice. The close correlation between the MAO activity and AD progress observed by *in vivo* monitoring for the first time prompts us to investigate the enzyme as a potential biomarker of AD.

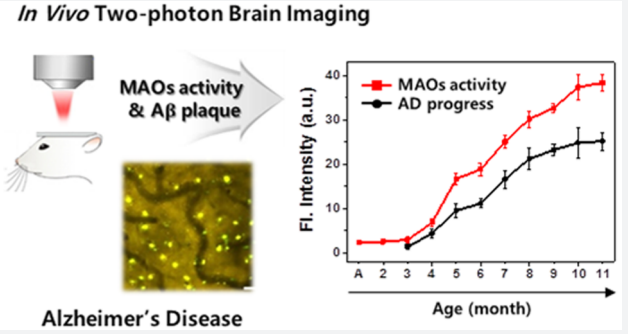

INTRODUCTION

Alzheimer's disease (AD), the most common form of dementia in the elderly, currently affects over 35 million people worldwide.[1] AD is known to be associated with multiple etiologies, including genetic vulnerability and environmental factors. Representative clinical symptoms of AD include irreversible memory loss, progressive cognitive decline, disorientation, language impairment, and emotional instability.[2] Currently, *in vitro* monitoring of AD is mostly conducted by biochemical examination of AD biomarkers such as amyloid-β (Aβ) peptides in the form of plaques (Aβ plaques) and intracellular neurofibrillary tangles of hyperphosphorylated tau (NFTs).[3,4] Assays of these two major neuropathological markers in the cerebrospinal fluid (CSF) seem to be promising, but such *in vitro* assays also raise questions in terms of accuracy and reliability for discrimination of the disease state.[5−7] Alternatively, *in vivo* diagnostic imaging methods for the key biomarkers are in clinical practice, which include PET (positron emission tomography), SPECT (single photon emission computed tomography), and MRI (magnetic resonance imaging).[8,9] Accordingly, several FDA-approved imaging agents are extensively used in clinical practice and in academia to understand AD-associated pathology.[10] These imaging methods, however, have high cost, limited accessibility, and time-consuming data processing procedures. Additionally, excessive exposure to damaging radiation is a concern with the PET/SPECT methods.[11] Finally, the relatively low resolution of these imaging techniques limits their ability to yield distinguishing morphological differences between normal and abnormal tissues. Therefore, there is a great demand for readily accessible, convenient, and sensitive diagnostics for AD, in particular by detecting potential AD biomarkers present outside the brain. Fluorescence microscopy provides a versatile means in neuroimaging of AD in animal models, as it offers high resolution, high sensitivity, low cost, broad availability, and real-time monitoring in various animals. Such properties offer precise and accurate data in investigating disease-related biological processes, in diagnosis and prognosis, and in drug discovery.[11,12] Among the various fluorescence imaging techniques, two-photon microscopy (TPM) has received increasing interest in recent years. TPM with near-infrared laser (NIR) light (700−1000 nm) allows focal point excitation and provides 3D images with excellent resolution, in addition to causing less photodamage and photobleaching needed for long-term imaging.[13,14] TPM using NIR light also alleviates the

Received: October 18, 2016
Published: December 7, 2016

DOI: 10.1021/acscentsci.6b00309
ACS Cent. Sci. 2016, 2, 967−975

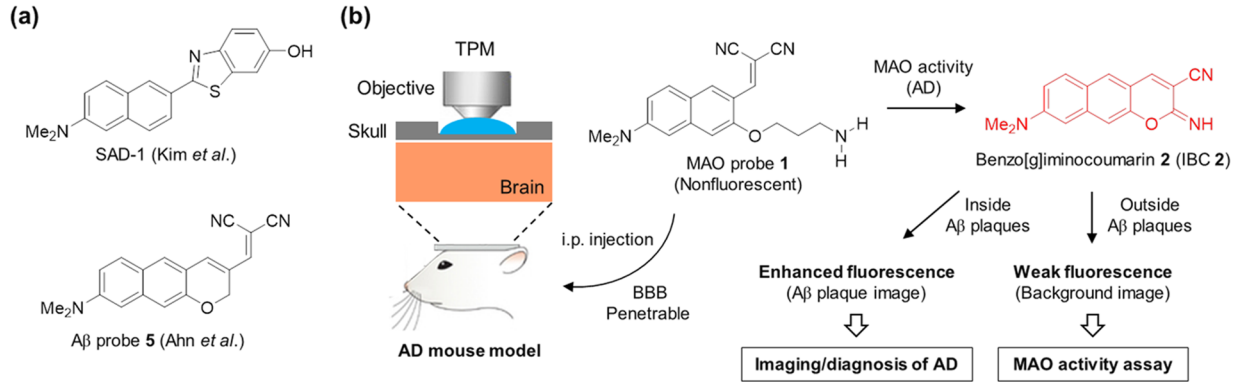

Figure 1. Chemical structures and an overall scheme for *in vivo* TPM imaging. (a) Chemical structures of SAD-1 and Aβ probe **5**. (b) *In vivo* coimaging scheme of MAO activity and Aβ plaques using probe **1** in live AD mouse model.

common interference from autofluorescence of intrinsic biomolecules during deep tissue imaging.[15] Accordingly, TPM has been widely used in preclinical research using animal models.[16,17]

Recently, a few two-photon probes for Aβ plaques have been reported (Figure 1a). SAD-1 (Kim et al., 2013)[18] and Aβ probe **5** (Ahn et al., 2015)[19] showed efficient *in vivo* TPM imaging capability toward Aβ plaques in a transgenic AD mouse model. In search of a convenient diagnostic for AD, we became interested in identifying biomarkers for AD other than Aβ plaques. Monoamine oxidases (MAO-A and MAO-B), which are known to be associated with AD, are such a candidate. MAOs are a family of FAD-dependent enzymes found in the outer mitochondrial membrane of neuronal, glial, and other mammalian cells.[20] MAOs catalyze the oxidative deamination of biogenic amines and play key roles in the metabolism of neurotransmitters in the central nervous system (CNS). Dysfunction of MAOs is closely associated with brain disorders such as AD, Parkinson's disease (PD),[21] and Huntington's disease (HD).[22] AD and PD are known to be associated with an elevated level of MAO-B in the cortical and hippocampal regions of brain.[23,24] MAO-B, the predominant isoform in human brain and mostly localized in glial cells, is known to be activated with age and in AD, although both the reason and the mechanism of its upregulation are not understood.[25] According to enzymatic radioimmunoassays performed on post-mortem human brain tissues, the increased MAO-B activity was ascribed to an increase in enzyme concentration.[26] The upregulated MAO-B level in AD patients may be due to increased gliosis, and it has been suggested that the elevated MAO-B activity in the aging brain and in AD may contribute to cellular degeneration by the overproduction of hydrogen peroxide, a byproduct of amine oxidation by the enzyme.[27] Treatment with a MAO-B inhibitor, L-deprenyl (also known as selegiline), improves PD and also appears to retard the cognitive decline in AD.[28] A growing body of evidence suggests that MAOs play a major role in aging as well as in age-related neurological diseases such as AD and PD.

The available evidence suggesting elevation of MAO activity with AD is all based on *in vitro* assays of sectioned brain tissues.[29,30] A direct correlation between MAO activity associated with AD from *in vivo* assays is lacking. *In vivo* monitoring of MAO activity as a function of AD progression, however, remains a challenging task. *In vivo* monitoring of MAO activity along with Aβ plaques is needed to assess their potential correlation. To date, two-photon probes with the capability to coimage *in vivo* Aβ plaques and potential AD biomarkers such as monoamine oxidase (MAOs),[31] β-site amyloid precursor protein cleaving enzyme (BACE),[32,33] or acetylcholine esterase[34] have not been explored. Unambigous correlation data on biomarkers associated with AD would provide valuable information in understanding the complex AD pathology and diagnosing its progression. In this work, we developed a probe that allows comonitoring of Aβ plaques and MAO activity in a mouse model of AD, establishing the first *in vivo* correlation between these two disease markers. We find that MAO activity increases as AD progresses, providing a solid path for potential diagnosis of AD.

RESULTS AND DISCUSSION

Comonitoring strategy. To correlate MAO activity along with the progress of AD by fluorescence TPM imaging, we focused on a two-photon probe for Aβ plaques that could be selectively activated by MAOs. Our earlier investigations identified MAO probe **1**, which generates benzo[*g*]imino-coumarin **2** (IBC **2**) as the product of enzymatic oxidation by MAO. IBC **2** is a flat and elongated dipolar dye which we reasoned might selectively sense Aβ plaques (Figure 1b), due to its structural similarity to the known probes.[35] Most of the known fluorescent probes for Aβ plaques also have a dipolar character, making them weakly emissive outside Aβ plaques but highly emissive inside Aβ plaques. It should be noted that although MAO-B is predominantly active in the brain and of most interest for AD diagnosis, probe **1** senses both MAO-A and MAO-B.

MAOs transform the aminopropyl moiety of probe **1**, which is nonfluorescent, into the corresponding iminium ion intermediate, which, upon hydrolysis followed by β-elimination, generates the corresponding hydroxy intermediate, which immediately condenses with one of the nitrile groups in **1** to produce a highly fluorescent IBC **2** as the final product (Figure S2). This turn-on type fluorescence response allowed us to selectively detect MAOs. Enzyme assays with probe **1** as MAO substrate gave a comparable level of K_m (Michaelis–Menten constant) and k_{cat} (turnover number) values for MAO-A (K_m = 70 μM, k_{cat} = 71 min^{-1}) and MAO-B (K_m = 75 μM, k_{cat} = 53 min^{-1}), determined in pH 7.4 HEPES buffer. In the case with natural amine substrates K_m values are in the μM range.[36] The enzymatic transformation of probe **1** into IBC **2** by MAOs is reasonably fast for bioimaging application: k_{obs} (observed rate constant with correlation factor $R^2 > 0.95$) = 5.8 s^{-1} (MAO-A) and 6.4 s^{-1} (MAO-B).

DOI: 10.1021/acscentsci.6b00309
ACS Cent. Sci. 2016, 2, 967–975

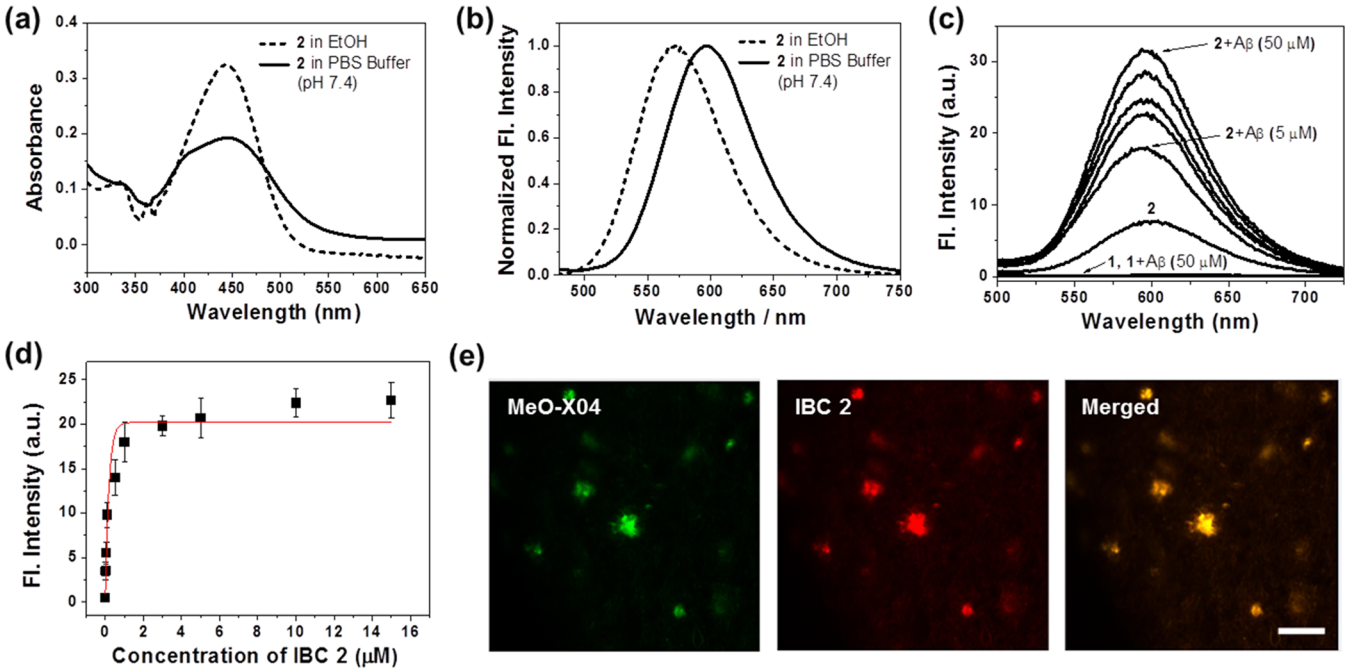

Figure 2. *In vitro* analysis of IBC **2**. (a, b) Absorption and emission spectra of IBC **2** (10 μM) in ethanol and PBS buffer (pH 7.4), respectively. (c) Fluorescence spectra of probe **1** (10 μM) and IBC **2** (10 μM) in the presence of Aβ plaques (0−50 μM) in PBS buffer (pH 7.4). (d) Saturation binding curve of Aβ plaques (10 μM) dependent on [IBC **2**] (0−15 μM) in PBS buffer (pH 7.4). The intensity represents the peak height at the maximum emission wavelength. All the measurements were conducted at 25 °C after 1 h of mixing under 450 nm excitation. (e) *In vitro* TPM images of Aβ plaques in the frontal cortex of 5XFAD mouse brain tissue costained with MeO-X04 (10 μM, 760 nm excitation, detection through green channel of 500 ± 30 nm) and IBC **2** (10 μM, 850 nm excitation, detection through red channel of 600 ± 30 nm) after 45 min incubation in aCSF. IBC **2** shows negligible fluorescence at 760 nm excitation (Figure S6). Imaging depth is at the middle of the tissue samples (~50 μm). Two-photon laser power was ~30 mW at the focal point. Scale bar is 20 μm.

IBC **2** has promising photophysical properties for the *in vivo* two-photon imaging application: It has (i) absorption and fluorescence emission bands in the biological transmission window[37] (one- and two-photon excitation at 450 nm and ~900 nm, respectively; emission at 600 nm with quantum yield of 0.63), (ii) sufficient two-photon absorbing property (TPACS = 180 GM),[36] (iii) a low molecular weight (MW = 263.10), and (iv) an optimal lipophilicity value required for BBB penetration: Log*P* values are 2.91 ± 0.94 for IBC **2** and 2.77 ± 0.80 for MAO probe **1**, as calculated by using ACDLab-ACDLogP software, from which Log*BB* values obtained are 0.97 for IBC **2** and 0.93 for MAO probe **1**. Log*BB* = (Log*P*−0.1725)/2.808.[38,39]

Upregulated MAO activity in AD mice is expected to generate a higher level of the enzyme reaction product, IBC **2**, in AD mice relative to healthy mice. IBC **2** is a typical donor (D)−acceptor (A) type dipolar dye, which has intramolecular charge transfer (ICT) excited states and is thus sensitive to the polarity of its surroundings. Thus, it emits weaker fluorescence in aqueous media (outside the plaques) but enhanced fluorescence in the hydrophobic and congested environment of Aβ plaques,[40] enabling their selective detection. The presence of IBC **2** outside Aβ plaques appears to give residual fluorescence whose intensity is dependent on MAO activity. Therefore, MAO activity could potentially be directly correlated with the progress of AD, by comonitoring the intensity and distribution of the signal from the free probe and from the probe bound to Aβ plaques (Figure 1b).

***In Vitro* Aβ Plaque Binding Assay of IBC 2.** We first monitored absorption and emission spectal changes of IBC **2** upon treatment with Aβ plaques, the results of which are given in Figure 2. IBC **2** exhibits an absorption maximum at 450 nm in either ethanol or PBS buffer (Figure 2a), and the fluorescence maxima appear at 571 nm and at 600 nm in ethanol and in PBS buffer, respectively (Figure 2b). The polarity inside Aβ plaques is similar to that of ethanol,[18] which suggests that a similar bathochromic shift in the emission wavelength should occur when IBC **2** is translocated into Aβ plaques. Indeed, an emission shift (10 nm) along with an intensity enhancement (>5-fold) was observed when IBC **2** was introduced to Aβ plaques (Figure 2c). The fluorescence enhancement is attributed to the more hydrophobic and congested environment inside Aβ plaques. In contrast, probe **1** showed no change in fluorescence in the presence of Aβ plaques only. The plaque-binding affinity of IBC **2** was measured by fluorescence titration over a wide range of Aβ plaque concentrations (Figure 2d, Figure S3), affording a dissociation constant of K_d = 32.2 ± 6.4 nM. The fluorescence titration data shows that 10 μM Aβ plaques accommodate 2 μM IBC **2** (5:1 binding stoichiometry), although such value is expected to be dependent on the size distribution and morphology of Aβ plaques prepared. The fluorescence spectrum of IBC **2** showed little depencence on medium, yielding comparable spectra in PBS buffer, in aCSF (artificial cerebrospinal fluid; see the composition in the Supporting Information), or in aCSF containing BSA (bovin serum albumin) (Figure S4). Also, the fluorescence emisison of IBC **2** is not influenced by AD-associated divalent metal ions such as Cu^{2+} and Zn^{2+} (Figure S4).[41]

***Ex Vivo* TPM Imaging of Aβ Plaques in Brain Tissues Using IBC 2.** To examine selective staining of Aβ plaques using IBC **2**, we conducted *ex vivo* TPM imaging of AD mouse brain

DOI: 10.1021/acscentsci.6b00309
ACS Cent. Sci. 2016, 2, 967−975

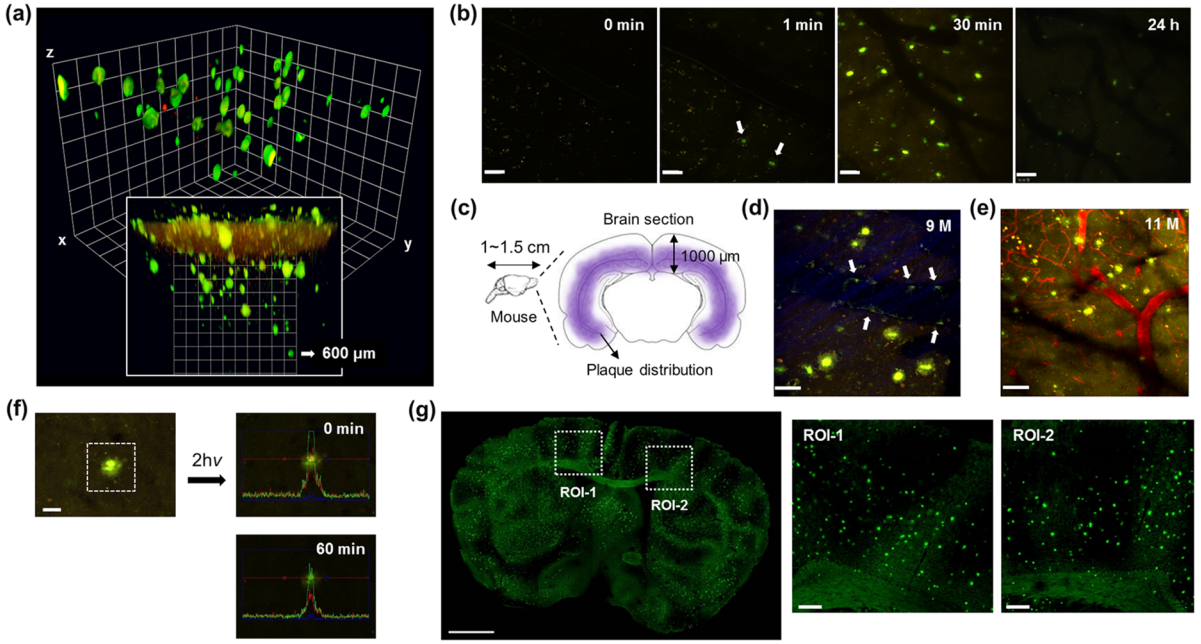

Figure 3. *In vivo* imaging of Aβ plaques using IBC **2**. (a) 3D-reconstructed, magnified (20×) fluorescence images of Aβ plaques in the frontal cortex of transgenic mouse (5XFAD, 9-month-old), obtained after ip injection of IBC **2** (10 mg kg^{-1}; 2 h circulation) by *in vivo* TPM under excitation at 850 nm with approximately 50 mW laser power at the focal point. Image reveals a plaque at 600 μm depth (along the *z*-direction) from the surface of the cortex. The fluorescence from both the green and red channels was collected. The unit scale is 45 μm. (b) *In vivo* fluorescence images of Aβ plaques in 5-month-old 5XFAD mouse after ip injection of IBC **2** (10 mg kg^{-1}), obtained by *in vivo* TPM at different time intervals (excitation at 850 nm; 50 mW laser power). Imaging depth was approximately 200 μm. Scale bar is 30 μm. (c) Illustration of brain section and plaque distribution. (d) CAA (cerebral amyloid angiopathy), observed near the blood vessel (the dark channel) as indicated by the white arrows from the *in vivo* TPM image of a 5XFAD (9-month-old) mouse brain. Imaging depth is 200 μm. Scale bar is 30 μm. (e) Snapshot of the video clip for Aβ plaques and blood vessel in 5XFAD (11-month-old) mouse brain, stained with IBC **2** and Dextran-Texas-Red (70 kDa, 25 mg kg^{-1} just before imaging), respectively. The emission from Dextran-Texas-Red was collected with >650 nm filter under two-photon excitation at 850 nm (50 mW). Scale bar is 50 μm. (f) *In vivo* two-photon laser photobleaching assay of a plaque stained with IBC **2** (10 mg kg^{-1}; 9-month-old 5XFAD mouse; after 2 h circulation) and located at approximately 50 μm depth. Two-photon laser (80 mW; 850 nm) was irradiated for 60 min. Fluorescence intensity was analyzed before and after 60 min in three different detection channels: green (green line, 500 ± 30 nm), red (red line, 600 ± 30 nm), and blue (blue line 420 ± 30 nm). The *x*-axis and *y*-axis represent pixels and fluorescence intensity, respectively. (g) Fluorescence OPM images for a sectioned brain tissue (*x*−*z* axis cut) isolated from a mouse after *in vivo* TPM imaging. Fluorescence was collected in the green channel (500 ± 30 nm) under excitation at 450 nm. Scale bar is 1000 μm. Two cortex regions in the rectangle are magnified (scale bar: 200 μm).

tissues after costaining with MeO-X04,[42,43] a reference staining dye for Aβ plaques. The brain tissue slices were prepared from a 9-month-old transgenic mouse (5XFAD, tg6799)[44] that had well-developed Aβ plaques. Brain hippocampal tissues were horizontally sectioned and then immersed in a solution containing both IBC **2** and MeO-X04 (10 μM for 45 min, respectively), which were then washed with aCSF medium prior to imaging (for details, see Supporting Information). Two-photon excitation at 850 nm provided the best image quality (see Figure S5 for screening of an optimal *in vivo* two-photon excitation wavelength). IBC **2** stained Aβ plaques with a strong red emission signal, which was colocalized with the reference dye, confirming that IBC **2** efficiently accumulates into and senses Aβ plaques (Figure 2e).

***In Vivo* TPM Imaging of Aβ Plaques in Live Mice Using IBC 2.** Given that IBC **2** showed an excellent ability to image Aβ plaques *in vitro*, we next performed *in vivo* imaging experiments of live AD mice by TPM. A 9-month-old 5XFAD AD mouse was anesthetized, and a cranial window was installed by thinned skull surgery (for details, see Supporting Information). IBC **2** was then injected intraperitoneally (10 mg kg^{-1}) into the mouse, and the distribution of Aβ plaques in the cortex region was monitored by two-photon excitation at 850 nm (~50 mW laser power at the focal point). IBC **2** was readily visualized in the Aβ plaques at depths >600 μm (Figure 3a), demonstrating the ability of IBC **2** to pass the blood−brain barrier relatively rapidly (for Aβ plaque staining after 1 min: Figure 3b, indicated by the white arrow). There was negligible fluorescence detected after 24 h (Figure 3b, Figure S7), indicating that the probe was rapidly cleared from the hippocampus. Notably, the imaging capability of IBC **2** is at least 2× deeper than that of previously reported two-photon probes for Aβ plaques.[18] It is known that Aβ plaques in 5XFAD mice first appear in the deeper layers of the cortex (>500 μm) and then gradually spread to the entire cortex near the skull surface (Figure 3c, the purple cloud indicates the main distribution of Aβ plaques).[45] Therefore, a dye that enables deeper tissue imaging is crucial for *in vivo* monitoring of AD progress. Furthermore, the surrounding blood vessels showed evidence of small amyloid deposits, which may be ascribed to the cerebral amyloid angiopathy (CAA)[46] (Figure 3d, indicated by the white arrow). This result also highlights the high sensitivity of IBC **2** for imaging of small amyloid deposits. Additionally, real-time monitoring of plaque staining was carried out by separate blood staining with Dextran-Texas-Red (Figure 3e, Figure S8, Supporting Movie S1). Such long-term *in vivo* monitoring was made possible by the high photostability of IBC **2**: When a selected Aβ plaque was irradiated with the two-photon laser for 60 min even under

DOI: 10.1021/acscentsci.6b00309
ACS Cent. Sci. 2016, 2, 967−975

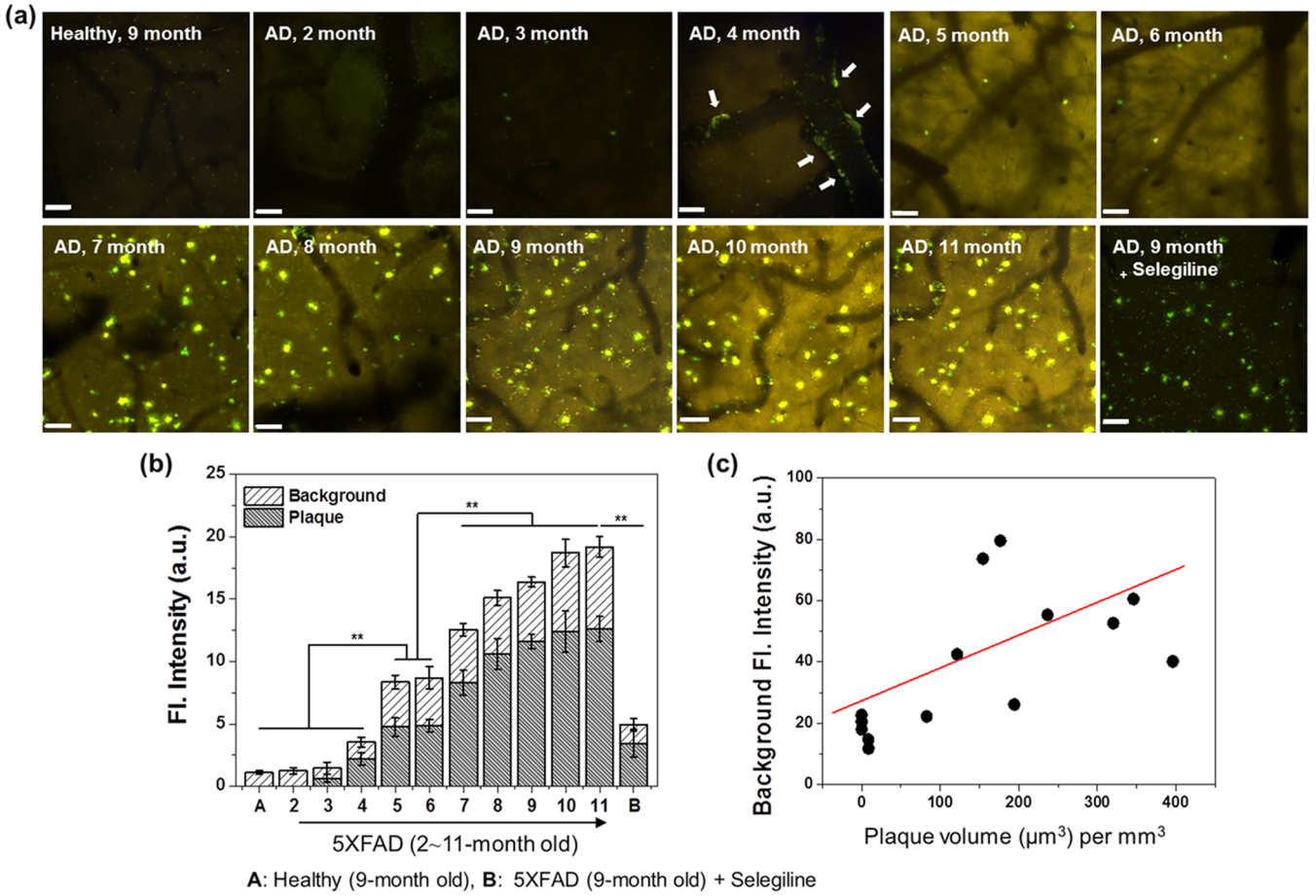

Figure 4. *In vivo* TPM coimaging of MAO activity and Aβ plaques using probe **1**. (a) *In vivo* fluorescence images (from *z*-stack, magnified 20×) of the frontal cortex region of transgenic (5XFAD, 2−11-month-old, n = 2−3) and healthy mice (9-month-old, n = 3), obtained after ip injection of probe **1** (10 mg kg^{-1}, 2 h circulation) by TPM under excitation at 850 nm with approximately 50 mW laser power at the focal point. The images were acquired at 200−300 μm depth (along the *z*-direction) from the surface of the cortex. The fluorescence from both the green and red channels was collected. The scale bar is 60 μm. (b) Plots of the average fluorescence intensity of Aβ plaques and background images in panel a, respectively (the background bar starts from the bottom). (c) A plot of the background fluorescence intensity versus the plaque volume (μm^3) per mm^3. Those values were obtained from the *in vivo* two-photon *z*-stacked images for the frontal cortex of 5XFAD AD mouse (2−11-month old, n = 5) treated with probe **1** (10 mg kg^{-1}, 2 h circulation). Each point indicates correlated average values of the background fluorescence intensity and the plaque volume, which were calculated using Zen 2011 software (Carl Zeiss Inc.) and Volocity software (PerkinElmer).

harsh conditions for organic molecules (850 nm; 80 mW), only 30% of the fluorescence signal was bleached (Figure 3f).

One-photon confocal microscope images were acquired on a brain tissue section to obtain a wide area image of Aβ plaques (Figure 3g). This image revealed the Aβ plaques to be distributed primarily in the 300−1000 μm outer edge of the cerebral cortex region (magnified image of white box in Figure 3g). The data show that the penetration depth obtained by two-photon imaging of IBC **2** is sufficient to reveal most of the plaque-related AD pathology in this model.

***In Vivo* TPM Comonitoring of MAO Activity and Aβ Plaques in Live Mice Using Probe 1.** Given that IBC **2** showed high sensitivity and fast response to Aβ plaques, we next investigated the ability of probe **1** to comonitor MAO activity and Aβ plaques *in vivo*. Probe **1** produces the Aβ plaque-imaging agent IBC **2** upon reaction with MAOs, and so probe **1** is a marker of both MAO activity and Aβ plaques. Probe **1** was intraperitoneally injected (10 mg kg^{-1}) to healthy (9-month-old, n = 3) and 5XFAD AD mice (2−11-month-old, n = 2−3), and then a cranial window was installed in each mouse using the protocol described above. A good cell viability of probe **1** was confirmed by a cellular metabolism assay.[36] After 2 h circulation of the probe, fluorescence images were acquired through the cranial window under two-photon excitation conditions. The fluorescence images, collected at 200−300 μm depth from a *z*-stack (Figure 4a), showed a distinct increase in the number and size of Aβ plaques as well as an increase in the background fluorescence signal associated with MAO activity as the mice aged and AD progressed. IBC **2** generated by MAO activity is responsible for both the "background" (outside plaques) and Aβ plaque signals. The fluorescence response was negligible in the healthy mice but significant in the 4-month-old AD mice, and the intensity became more substantial in the older mice. Moreover, CAA species appeared in the 4-month-old mice (Figure 4a, indicated by the white arrow). Large Aβ plaques became abundant in the 7-month-old mice. Additionally, we noted substantial spreading of the plaques through the entire cortex at the later stages of AD.

The fluorescence intensity of the background region and in the Aβ plaques was extracted separately from the imaging data by choosing suitable threshold values, which was plotted as the bar graph shown in Figure 4b. Both the background signal and the plaque signal gradually increased as the age of the mice

DOI: 10.1021/acscentsci.6b00309
ACS Cent. Sci. 2016, 2, 967−975

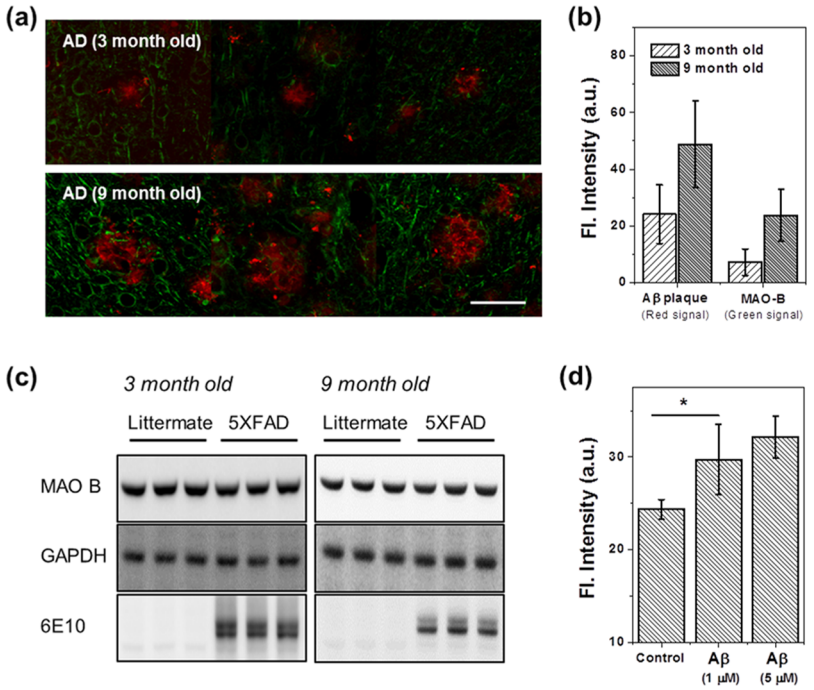

Figure 5. Histological staining of MAOs and their activity associated with Aβ plaques. (a) Histological staining of brain slices in the frontal cortex of transgenic mouse (5XFAD, 3- and 9-month-old, n = 3 for each sample) costained with a MAO-B antibody (excitation at 499 nm; detection at 500−550 nm) and MeO-X04 (10 μM; excitation at 400 nm and detection at 420−500 nm, red pseudocolored to improve the contrast). Scale bar is 20 μm. (b) Relative fluorescence intensity of Aβ plaques (red-colored, imaged with MeO-X04) and MAO-B (green-colored, imaged with MAO-B antibody) shown in panel a. The relative intensity and standard deviation were calculated using ImageJ software (NIH, USA) at 10 different ROIs (area: 50 μm^2) on the red and green signal region, respectively. (c) Western blots of MAO-B concentration for the brain tissue samples of healthy (littermate; 3- and 9-month-old, n = 3, respectively) and 5XFAD (3- and 9-month-old, n = 3, respectively) mice. GAPDH is a loading control for the blot. (d) Activity assay of MAO-B in U373 astrocytoma cells treated with $A\beta_{1-42}$ peptide (1 μM and 5 μM, respectively). Control: without Aβ peptide. The fluorescence intensity corresponded to the H_2O_2 concentration, a side product of MAO's catalytic action (see Supporting Information for the experimental protocol).

increased, suggestive of a close correlation. Also, the background fluorescence intensity with respect to the plaque volume shows a rough but apparent proportionality (Figure 4c, 2−11-month-old 5XFAD mice, n = 5, number of z-stacked images = 15). The *in vivo* coimaging data unambiguously establish that MAO activity increases as AD progresses. It should be noted that the background signal only approximately represents the MAO activity, because it does not account for the quantity of IBC **2** taken up by the Aβ plaques. This quantity scales with the number and the volume of Aβ plaques, which depend on the age of the animal. The total volume of plaques is much less than that of the background region. If we assume that the concentration of IBC **2** in the plaques is not much greater than that in the background region, we can estimate that the background signal represents most of the IBC **2** produced by enzymatic activity. The close correlation between the background signal and the plaque signal thus indicates that MAO activity is highly correlated with the progress of AD. Figure 4b shows that the progress of AD can be categorized into three stages: a slow initiation stage up to three months, a subsequent aggressive stage, and then a saturation stage after nine months. Above all, the *in vivo* correlation between MAO activity and AD progress suggests that monitoring of MAO activity may be an alternate means to follow the progress of AD. The production of IBC **2** in the AD mouse brain was confirmed by MALDI-TOF analysis of the chemical extracts isolated from the brain (see Methods in Supporting Information) (Figure S10).

We further conducted control experiments with the late stage AD mice (9-month-old, n = 3) that were fed a MAO inhibitor, selegiline.[47] In this case, we observed significantly reduced signal both from the background and from the plaques, indicative of reduced production of IBC **2** due to inhibition of MAO activity (Figure 4, Figure S11).

Histological Staining of MAOs and Their Activity Associated with Aβ Plaques. Along with the *in vivo* imaging, we also conducted *ex vivo* assays of MAOs and Aβ plaques in the 5XFAD mouse brain by histological tissue staining. We mainly analyzed MAO-B activity because it is the major isoenzyme in AD pathology.[31] Each of the sectioned brain tissues (3- and 9-month-old) was incubated with a primary MAO-B antibody followed by an Alexa Fluoro 488 dye-conjugated secondary antibody (λ_{em} = 500−550 nm, green) for staining MAO-B. At the same time, MeO-X04 (λ_{em} = 420−500 nm) was used to stain the Aβ plaques, whose images were pseudocolored in red to improve the contrast. The costaining results showed bright green fluorescence responsible for the quantity of MAO-B around Aβ plaques (Figure 5a). Both the green and red images became brighter (2−3 times) in the sample from the older mouse (Figure 5b), indicative of a higher level of MAO-B in the aged/AD-progressed mouse.

Next, we quantified the total concentration of MAO-B by Western blot analysis. The blots of brain tissue samples from healthy and 5XFAD mice (3- and 9-month-old, n = 3, respectively) were incubated with primary antibodies (anti-Aβ, anti-MAO-B, anti-GAPDH) and consequent secondary antibodies. Interestingly, the results indicated that there was no significant difference in the MAO-B concentration in either the healthy or the AD mice (Figure 5c, Figure S12). According to

DOI: 10.1021/acscentsci.6b00309
ACS Cent. Sci. 2016, 2, 967−975

previous enzymatic radioimmunoassays performed on post-mortem human brain tissues, the increased MAO-B activity in AD patients was ascribed to an increase in enzyme concentration, not to elevated enzyme activity.[26] Our *in vivo* assays in the mouse model suggest that not only the local concentration of MAO-B but also its activity increase as AD progresses.

We also checked the elevation of MAO activity in the presence of Aβ peptides. U373 human astrocytoma cells were treated with Aβ peptides at different concentations (fragment 1−42),[48] and MAO activity was followed by fluorimetric monitoring of H_2O_2, generated as a side product of the enzymatic oxidative deamination. The results showed a substantial increase in MAO activity in the presence of Aβ peptides, in corroboration with the previous report[49,50] (Figure 5d for MAO-B activity assay, Figure S13 for MAO-A/B activity assay). Thus, we conclude that the accumulation of MAOs around Aβ plaques causes activation of the enzyme, which becomes more active as AD progresses.

CONCLUSION

In conclusion, *in vivo* comonitoring of MAO activity along with amyloid-β plaques in live mice with AD was demonstrated for the first time. A reaction-based two-photon MAO probe enabled this comonitoring, as its enzyme reaction product can pass the blood−brain barrier and sense amyloid-β plaques to a depth of 600 μm. The *in vivo* deep-tissue imaging results showed a distinctive age-dependent fluorescence increment for both amyloid-β plaques and an increase in the background enzymatic activity (outside the plaques). The close correlation categorizes the progress of AD in mice into three apparent stages: a slow initiation stage from birth to three months, a subsequent aggressive stage, and then a saturation stage after nine months. Histological staining data showed greater enzyme activity around Aβ plaques in aged AD mice. The close *in vivo* correlation between MAO activity and progress of AD indicates that further investigation of the enzyme as a potential biomarker of AD is warranted.

METHODS

General Information. The chemical reagents were purchased from Aldrich or TCI. Commercially available reagents were used without further purification. Anhydrous solvents for organic synthesis were prepared by passing through a solvent purification tower. All reactions were performed under argon atmosphere unless otherwise stated. Thin-layer chromatography (TLC) was performed on precoated silica gel 60F-254 glass plates. UV/vis absorption spectra were obtained using a HP 8453 UV/vis spectrophotometer. Fluorescence emission spectra were recorded on a PTI (Photon Technical International) fluorescence system using a 1 cm standard quartz cell.

***In Vitro* Assay of Probe 1 and IBC 2.** Aβ42 (Sigma-Aldrich, A9810, molecular weight = 4514.04, 1 mg) was dissolved in PBS buffer (10 mM, pH 7.4) to a final concentration of 100 μM. This solution was incubated in an e-tube shaker (60 rpm, F1 mode of SLRM-2M, MyLab Corp.) at 25 °C for 3 days, and used for *in vitro* assay directly. Incubation of aggregated Aβ with probe **1** or IBC **2** was carried out under the same incubating conditions for 1 h. A stock solution (10 mg mL^{-1}) of bovine serum albumin (BSA, Promega, R396D) was prepared in PBS buffer (10 mM, pH 7.4). The composition of artificial cerebrospinal fluid (aCSF) was NaCl (124 mM), KCl (3 mM), NaH_2PO_4 (1.25 mM), $MgCl_2$ (1 mM), $NaHCO_3$ (36 mM), D-glucose (10 mM), $CaCl_2$ (2 mM), 95% O_2, and 5% CO_2 (by bubbler).

5XFAD Transgenic Mice. 3−11-month-old 5XFAD Tg mice (Tg6799, Stock No. 006554) purchased from The Jackson Laboratory (Bar Harbor, ME) were used for *ex vivo*/*in vivo* one-photon/two-photon imaging, immunohistochemistry, and Western blot experiments. Five mutations, human APP 695 (Swedish, Florida, and London) and human Presenilin 1 (M146L and L286 V), related with familial Alzheimer's disease (FAD) were expressed in 5XFAD mice. With these mutants, 5XFAD mice produced amyloid-β 42 (Aβ42) rapidly and accordingly amyloid plaques appeared from 2-month-old mouse in the frontal cortex (layer 5) and the subiculum. Especially in the frontal cortex, amyloid plaques were spread from layer 5 to layer 1 as growing. Neuronal cell deaths and glial cell activations were also detected with deposits of plaques.[45] Animal maintenance and experiments were conducted under "the Animal Care and Use Guidelines of Seoul National University".

***Ex Vivo* TPM Imaging.** 5XFAD Tg mice were sacrificed by cervical dislocation, and the brain was immediately extracted. The isolated brain was fixed in a stage of vibrating blade microtome (Leica, Nussloch, Germany) filled with artificial cerebrospinal fluid (aCSF) with oxygen bubbling (95% O_2, 5% CO_2). Horizontally sectioned brain hippocampal tissues were immersed in a solution containing IBC **2** (10 μM) and Methoxy-X04 (10 μM) for 45 min in the living stage, and then they were washed with aCSF. During two-photon imaging, aCSF (95% O_2, 5% CO_2) was continuously supplied at 33 °C to tissues using a peristaltic pump (Gilson Inc., Middleton, WI, USA) with a fluidic inline heater (Live cell instrument, Seoul, Korea).

Thinned Skull Surgery. Thinned skull surgery was performed for *in vivo* two-photon imaging. Anesthetized mice with the mixture of Zoletil 50 (Virbac, Carros, France) and Rompun (Bayer Korea, Seoul, Korea) (1.2 mL kg^{-1}, intramuscular injection) were fixed on a customized heating plate (37 °C; Live cell instrument, Seoul, Korea). Subsequently, dexamethasone (0.2 mg kg^{-1}, im) was injected to prevent inflammation. The mouse scalp was sterilized with ethanolic water (70%). A region of 0.5−1 mm relative to bregma was chosen, and the skull was ground smoothly with a microdrill down to the skull depth of about 30 μm. When the surgery was completed, we dropped cyanoacrylate and attached a round coverslip (5 mm). Lastly dental cement was applied to the emerged region.

***In Vivo* TPM Imaging.** Two-photon microscopy (LSM 7 MP; Carl Zeiss Inc., Goettingen, Germany) equipped with titanium−sapphire femtosecond laser (Chameleon Ultra; Coherent, Santa Clara, CA), and 20× water immersion objective lens (W Plan-Apochromat 20×/1.0 DIC M27 70 mm, Carl Zeiss Inc. Germany) was used for *in vivo* imaging. Probe **1** or IBC **2** was intraperitoneally injected (10 mg kg^{-1}) into mice (2−11-month-old 5XFAD Tg mice and 9-month-old litter mates (WT)) 2 h before imaging. In addition, Dextran-Texas-Red (70 kDa) was intravenously injected for blood vessel staining (25 mg kg^{-1}) just before imaging. The laser power was limited to 70 mW to avoid the damage associated with phototoxicity for *in vivo* mouse brain imaging as well as to minimize autofluorescence from tissues. Zen 2011 software

DOI: 10.1021/acscentsci.6b00309
ACS Cent. Sci. 2016, 2, 967−975

(Carl Zeiss Inc.) and Volocity software (PerkinElmer) were used for image analysis and 3D-reconstructed images.

MAO Inhibition Assay with Selegiline. A group of AD mice (9−10-month old, n = 3, respectively) were treated with selegiline (MAO inhibitor, 10 mg/150 mL in water, 1 week, *ad libitum*).[48] Imaging experiments were conducted by following the same protocol used for the *in vivo* two-photon imaging. P-value: * <0.05, ** <0.01, *** <0.001, n = 3−4 per group.

■ ASSOCIATED CONTENT

Supporting Information

The Supporting Information is available free of charge on the ACS Publications website at DOI: 10.1021/acscentsci.6b00309.

Experimental details and supporting figures (PDF)
In vivo two-photon brain imaging (AVI)

■ AUTHOR INFORMATION

Corresponding Authors

*E-mail: inhee@snu.ac.kr.
*E-mail: ahn@postech.ac.kr.

ORCID

Dokyoung Kim: 0000-0002-7756-3560
Michael J. Sailor: 0000-0002-4809-9826
Kyo Han Ahn: 0000-0001-7192-7215

Author Contributions

§D.K. and S.H.B. contributed equally.

Notes

The authors declare the following competing financial interest(s): The authors are listed as inventors on a pending patent application related to technology described in this work.

■ ACKNOWLEDGMENTS

This work was supported by Ministry of Health & Welfare (HI13C1378) and through National Research Foundation of Korea (NRF, 2014K1A1A2064569) funded by Ministry of Science, ICT & Future Planning. I.M.-J. thanks NRF for financial support (2015R1A2A1A05001794, 2014M3C7A1046047, 2015M3C7A1028790, MRC [2012R1A5A2A44671346]). D.K. is thankful for the financial support from UCSD Frontiers of Innovation Scholars Program (FISP) fellowship and Basic Science Research Program through the National Research Foundation of Korea (NRF) funded by the Ministry of Education (2016R1A6A3A-03006343).

■ REFERENCES

(1) Masters, C. L.; Bateman, R.; Blennow, K.; Rowe, C. C.; Sperling, R. A.; Cummings, J. L. Alzheimer's disease. *Nat. Rev. Dis. Primers* **2015**, 15056.

(2) Querfurth, H. W.; LaFerla, F. M. Alzheimer's disease. *N. Engl. J. Med.* **2010**, *362*, 329−344.

(3) Mattson, M. P. Pathways towards and away from Alzheimer's disease. *Nature* **2004**, *430*, 631−639.

(4) Goedert, M.; Spillantini, M. G. A century of Alzheimer's disease. *Science* **2006**, *314*, 777−781.

(5) Humpel, C. Identifying and validating biomarkers for Alzheimer's disease. *Trends Biotechnol.* **2011**, *29*, 26−32.

(6) Hampel, H.; Frank, R.; Broich, K.; Teipel, S. J.; Katz, R. G.; Hardy, J.; Herholz, K.; Bokde, A. L. W.; Jessen, F.; Hoessler, Y. C.; Sanhai, W. R.; Zetterberg, H.; Woodcock, J.; Blennow, K. Biomarkers for Alzheimer's disease: academic, industry and regulatory perspectives. *Nat. Rev. Drug Discovery* **2010**, *9*, 560−574.

(7) Lockhart, A. Imaging Alzheimer's disease pathology: one target, many ligands. *Drug Discovery Today* **2006**, *11*, 1093−1099.

(8) Johnson, K. A.; Fox, N. C.; Sperling, R. A.; Klunk, W. E. Brain imaging in Alzheimer disease. *Cold Spring Harbor Perspect. Med.* **2012**, *2*, a006213.

(9) Amiri, H.; Saeidi, K.; Borhani, P.; Manafirad, A.; Ghavami, M.; Zerbi, V. Alzheimer's disease: pathophysiology and applications of magnetic nanoparticles as MRI theranostic agents. *ACS Chem. Neurosci.* **2013**, *4*, 1417−1429.

(10) Garber, K. First FDA-approved beta-amyloid diagnostic hits the market. *Nat. Biotechnol.* **2012**, *30*, 575−575.

(11) Staderini, M.; Martin, M. A.; Bolognesi, M. L.; Menendez, J. C. Imaging of β-amyloid plaques by near infrared fluorescent tracers: a new frontier for chemical neuroscience. *Chem. Soc. Rev.* **2015**, *44*, 1807−1819.

(12) Tong, H.; Lou, K.; Wang, W. Near-infrared fluorescent probes for imaging of amyloid plaques in Alzheimers disease. *Acta Pharm. Sin. B* **2015**, *5*, 25−33.

(13) Helmchen, F.; Denk, W. Deep tissue two-photon microscopy. *Nat. Methods* **2005**, *2*, 932−940.

(14) Zipfel, W. R.; Williams, R. M.; Webb, W. W. Nonlinear magic: multiphoton microscopy in the biosciences. *Nat. Biotechnol.* **2003**, *21*, 1369−1377.

(15) Kim, D.; Ryu, H. G.; Ahn, K. H. Recent development of two-photon fluorescent probes for bioimaging. *Org. Biomol. Chem.* **2014**, *12*, 4550−4566.

(16) Delatour, B.; Epelbaum, S.; Petiet, A.; Dhenain, M. In vivo imaging biomarkers in mouse models of Alzheimer's disease: are we lost in translation or breaking through? *Int. J. Alzheimer's Dis.* **2010**, *2010*, 604853.

(17) Dong, J.; Revilla-Sanchez, R.; Moss, S.; Haydon, P. G. Multiphoton in vivo imaging of amyloid in animal models of Alzheimer's disease. *Neuropharmacology* **2010**, *59*, 268−275.

(18) Heo, C. H.; Kim, K. H.; Kim, H. J.; Baik, S. H.; Song, H.; Kim, Y. S.; Lee, J.; Mook-jung, I.; Kim, H. M. A two-photon fluorescent probe for amyloid-beta plaques in living mice. *Chem. Commun.* **2013**, *49*, 1303−1305.

(19) Kim, D.; Moon, H.; Baik, S. H.; Singha, S.; Jun, Y. W.; Wang, T.; Kim, K. H.; Park, B. S.; Jung, J.; Mook-Jung, I.; Ahn, K. H. Two-Photon absorbing dyes with minimal autofluorescence in tissue imaging: application to in vivo imaging of amyloid-beta plaques with a negligible background signal. *J. Am. Chem. Soc.* **2015**, *137*, 6781−6789.

(20) Edmondson, D. E.; Binda, C.; Wang, J.; Upadhyay, A. K.; Mattevi, A. Molecular and mechanistic properties of the membrane-bound mitochondrial monoamine oxidases. *Biochemistry* **2009**, *48*, 4220−4230.

(21) Li, L.; Zhang, C. W.; Chen, G. Y.; Zhu, B.; Chai, C.; Xu, Q. H.; Tan, E. K.; Zhu, Q.; Lim, K. L.; Yao, S. Q. A sensitive two-photon probe to selectively detect monoamine oxidase B activity in Parkinson's disease models. *Nat. Commun.* **2014**, *5*, 3276.

(22) Bortolato, M.; Chen, K.; Shih, J. C. Monoamine oxidase inactivation: from pathophysiology to therapeutics. *Adv. Drug Delivery Rev.* **2008**, *60*, 1527−1533.

(23) Youdim, M. B. H.; Bakhle, Y. S. Monoamine oxidase: isoforms and inhibitors in Parkinson's disease and depressive illness. *Br. J. Pharmacol.* **2006**, *147*, S287−S296.

(24) Adolfsson, R.; Gottfries, C. G.; Oreland, L.; Wiberg, Å.; Winblad, B. Increased activity of brain and platelet monoamine oxidase in dementia of Alzheimer type. *Life Sci.* **1980**, *27*, 1029−1034.

(25) Saura, J.; Bleuel, Z.; Ulrich, J.; Mendelowitsch, A.; Chen, K.; Shih, J. C.; Malherbe, P.; DaPrada, M.; Richards, J. G. Molecular neuroanatomy of human monoamine oxidases A and B revealed by quantitative enzyme radioautography and in situ hybridization histochemistry. *Neuroscience* **1996**, *70*, 755−774.

(26) Saura, J.; Luque, J. M.; Cesura, A. M.; Da Prada, M.; Chanpalay, V.; Huber, G.; Loffler, J.; Richards, J. G. Increased monoamine-xxidase-B activity in plaque-associated astrocytes of Alzheimer brains revealed by quantitative enzyme autoradiography. *Neuroscience* **1994**, *62*, 15−30.

DOI: 10.1021/acscentsci.6b00309
ACS Cent. Sci. 2016, 2, 967−975

(27) Riederer, P.; Danielczyk, W.; Grunblatt, E. Monoamine oxidase-B inhibition in Alzheimer's disease. *NeuroToxicology* **2004**, *25*, 271−277.
(28) Gulyas, B.; Pavlova, E.; Kasa, P.; Gulya, K.; Bakota, L.; Varszegi, S.; Keller, E.; Horvath, M. C.; Nag, S.; Hermecz, I.; Magyar, K.; Halldin, C. Activated MAO-B in the brain of Alzheimer patients, demonstrated by [11C]-L-deprenyl using whole hemisphere autoradiography. *Neurochem. Int.* **2011**, *58*, 60−68.
(29) Kumar, M. J.; Andersen, J. K. Perspectives on MAO-B in aging and neurological disease. *Mol. Neurobiol.* **2004**, *30*, 77−89.
(30) Reinikainen, K. J.; Paljarvi, L.; Halonen, T.; Malminen, O.; Kosma, V.-M.; Laakso, M.; Riekkinen, P. J. Dopaminergic system and monoamine oxidase-B activity in Alzheimer's Disease. *Neurobiol. Aging* **1988**, *9*, 245−252.
(31) Youdim, M. B. H.; Edmondson, D.; Tipton, K. F. The therapeutic potential of monoamine oxidase inhibitors. *Nat. Rev. Neurosci.* **2006**, *7*, 295−309.
(32) Ghosh, A. K.; Osswald, H. L. BACE1 (β-secretase) inhibitors for the treatment of Alzheimer's disease. *Chem. Soc. Rev.* **2014**, *43*, 6765−6813.
(33) Evin, G.; Barakat, A.; Masters, C. L. BACE: Therapeutic target and potential biomarker for Alzheimer's disease. *Int. J. Biochem. Cell Biol.* **2010**, *42*, 1923−1926.
(34) McGleenon, B. M.; Dynan, K. B.; Passmore, A. P. Acetylcholinesterase inhibitors in Alzheimer's disease. *Br. J. Clin. Pharmacol.* **1999**, *48*, 471−480.
(35) Staderini, M.; Martin, M. A.; Bolognesi, M. L.; Menendez, J. C. Imaging of [small beta]-amyloid plaques by near infrared fluorescent tracers: a new frontier for chemical neuroscience. *Chem. Soc. Rev.* **2015**, *44*, 1807−1819.
(36) Kim, D.; Sambasivan, S.; Nam, H.; Kim, K. H.; Kim, J. Y.; Joo, T.; Lee, K. H.; Kim, K. T.; Ahn, K. H. Reaction-based two-photon probes for in vitro analysis and cellular imaging of monoamine oxidase activity. *Chem. Commun.* **2012**, *48*, 6833−6835.
(37) Joshi, B. P.; Wang, T. D. Exogenous molecular probes for targeted imaging in cancer: focus on multi-modal imaging. *Cancers* **2010**, *2*, 1251−1287.
(38) Leeson, P. Drug discovery: Chemical beauty contest. *Nature* **2012**, *481*, 455−456.
(39) Carpenter, T. S.; Kirshner, D. A.; Lau, E. Y.; Wong, S. E.; Nilmeier, J. P.; Lightstone, F. C. A Method to Predict Blood-Brain Barrier Permeability of Drug-Like Compounds Using Molecular Dynamics Simulations. *Biophys. J.* **2014**, *107*, 630−641.
(40) Singha, S.; Kim, D.; Roy, B.; Sambasivan, S.; Moon, H.; Rao, A. S.; Kim, J. Y.; Joo, T.; Park, J. W.; Rhee, Y. M.; Wang, T.; Kim, K. H.; Shin, Y. H.; Jung, J.; Ahn, K. H. A structural remedy toward bright dipolar fluorophores in aqueous media. *Chem. Sci.* **2015**, *6*, 4335−4342.
(41) Faller, P.; Hureau, C. Bioinorganic chemistry of copper and zinc ions coordinated to amyloid-beta peptide. *Dalton Trans.* **2009**, 1080−1094.
(42) Klunk, W. E.; Bacskai, B. J.; Mathis, C. A.; Kajdasz, S. T.; McLellan, M. E.; Frosch, M. P.; Debnath, M. L.; Holt, D. P.; Wang, Y.; Hyman, B. T. Imaging Aβ plaques in living transgenic mice with multiphoton microscopy and Methoxy-X04, a systemically administered Congo Red derivative. *J. Neuropathol. Exp. Neurol.* **2002**, *61*, 797−805.
(43) McCarter, J. F.; Liebscher, S.; Bachhuber, T.; Abou-Ajram, C.; Hubener, M.; Hyman, B. T.; Haass, C.; Meyer-Luehmann, M. Clustering of plaques contributes to plaque growth in a mouse model of Alzheimer's disease. *Acta Neuropathol.* **2013**, *126*, 179−188.
(44) Morrissette, D. A.; Parachikova, A.; Green, K. N.; LaFerla, F. M. Relevance of transgenic mouse models to human Alzheimer disease. *J. Biol. Chem.* **2009**, *284*, 6033−6037.
(45) Oakley, H.; Cole, S. L.; Logan, S.; Maus, E.; Shao, P.; Craft, J.; Guillozet-Bongaarts, A.; Ohno, M.; Disterhoft, J.; Van Eldik, L.; Berry, R.; Vassar, R. Intraneuronal beta-amyloid aggregates, neurodegeneration, and neuron loss in transgenic mice with five familial Alzheimer's disease mutations: potential factors in amyloid plaque formation. *J. Neurosci.* **2006**, *26*, 10129−10140.
(46) Yamada, M. Cerebral amyloid angiopathy: An overview. *Neuropathology* **2000**, *20*, 8−22.
(47) Fowler, J. S.; Logan, J.; Volkow, N. D.; Shumay, E.; McCall-Perez, F.; Jayne, M.; Wang, G.-J.; Alexoff, D. L.; Apelskog-Torres, K.; Hubbard, B.; Carter, P.; King, P.; Fahn, S.; Gilmor, M.; Telang, F.; Shea, C.; Xu, Y.; Muench, L. Evidence that formulations of the selective MAO-B inhibitor, Selegiline, which bypass first-pass metabolism, also inhibit MAO-A in the human brain. *Neuropsychopharmacology* **2015**, *40*, 650−657.
(48) Jo, S.; Yarishkin, O.; Hwang, Y. J.; Chun, Y. E.; Park, M.; Woo, D. H.; Bae, J. Y.; Kim, T.; Lee, J.; Chun, H.; Park, H. J.; Lee, D. Y.; Hong, J.; Kim, H. Y.; Oh, S.-J.; Park, S. J.; Lee, H.; Yoon, B.-E.; Kim, Y.; Jeong, Y.; Shim, I.; Bae, Y. C.; Cho, J.; Kowall, N. W.; Ryu, H.; Hwang, E.; Kim, D.; Lee, C. J. GABA from reactive astrocytes impairs memory in mouse models of Alzheimer's disease. *Nat. Med.* **2014**, *20*, 886−896.
(49) Song, W.; Zhou, L. J.; Zheng, S. X.; Zhu, X. Z. Amyloid-beta 25−35 peptide induces expression of monoamine oxidase B in cultured rat astrocytes. *Acta Pharmacol. Sin.* **2000**, *21*, 557−563.
(50) Canobbio, I.; Abubaker, A. A.; Visconte, C.; Torti, M.; Pula, G. Role of amyloid peptides in vascular dysfunction and platelet dysregulation in Alzheimer's disease. *Front. Cell. Neurosci.* **2015**, *9*, 65.

DOI: 10.1021/acscentsci.6b00309
ACS Cent. Sci. 2016, 2, 967−975